

Geochemistry, Geophysics, Geosystems

RESEARCH ARTICLE

10.1002/2015GC005769

Key Points:

- Volcanic-arc-related hydrothermal site Palinuro exhibits a magnetization low
- This magnetic signature is comparable to that of basalt-hosted MOR sites
- Nonmagnetic hydrothermal deposit and alteration at depth are the major causes

Correspondence to:

F. Szitkar,
fszitkar@geomar.de

Citation:

Szitkar, F., S. Petersen, F. Caratori Tontini, and L. Cocchi (2015), High-resolution magnetics reveal the deep structure of a volcanic-arc-related basalt-hosted hydrothermal site (Palinuro, Tyrrhenian Sea), *Geochem. Geophys. Geosyst.*, 16, 1950–1961, doi:10.1002/2015GC005769.

Received 4 FEB 2015

Accepted 15 MAY 2015

Accepted article online 21 MAY 2015

Published online 26 JUN 2015

High-resolution magnetics reveal the deep structure of a volcanic-arc-related basalt-hosted hydrothermal site (Palinuro, Tyrrhenian Sea)

Florent Szitkar¹, Sven Petersen¹, Fabio Caratori Tontini², and Luca Cocchi³

¹Geomar Helmholtz Centre for Ocean Research, Kiel, Germany, ²GNS Science, Lower Hutt, New Zealand, ³Istituto Nazionale di Geofisica e Vulcanologia, Roma 2, U.P. Geofisica e Tecnologie Marine, Fezzano, SP, Italy

Abstract High-resolution magnetic surveys have been acquired over the partially sedimented Palinuro massive sulfide deposits in the Aeolian volcanic arc, Tyrrhenian Sea. Surveys flown close to the seafloor using an autonomous underwater vehicle (AUV) show that the volcanic-arc-related basalt-hosted hydrothermal site is associated with zones of lower magnetization. This observation reflects the alteration of basalt affected by hydrothermal circulation and/or the progressive accumulation of a nonmagnetic deposit made of hydrothermal and volcaniclastic material and/or a thermal demagnetization of titanomagnetite due to the upwelling of hot fluids. To discriminate among these inferences, estimate the shape of the nonmagnetic deposit and the characteristics of the underlying altered area—the stockwork—we use high-resolution vector magnetic data acquired by the AUV *Abyss* (GEOMAR) above a crater-shaped depression hosting a weakly active hydrothermal site. Our study unveils a relatively small nonmagnetic deposit accumulated at the bottom of the depression and locked between the surrounding volcanic cones. Thermal demagnetization is unlikely but the stockwork extends beyond the limits of the nonmagnetic deposit, forming lobe-shaped zones believed to be a consequence of older volcanic episodes having contributed in generating the cones.

1. Introduction

After the discovery of a magnetic low at the TAG hydrothermal site on the Mid-Atlantic Ridge [Tivey *et al.*, 1993], deep-sea, high-resolution magnetic exploration has confirmed that basalt-hosted hydrothermal sites along mid-ocean ridges are associated with a negative reduced-to-the-pole (RTP) magnetic anomaly, i.e., a weaker or missing magnetization [Tivey *et al.*, 1993; Tivey and Johnson, 2002; Tivey and Dymant, 2010; Zhu *et al.*, 2010; Caratori Tontini *et al.*, 2012a; Nakamura *et al.*, 2013; Honsho *et al.*, 2013; Szitkar *et al.*, 2014]. At active basalt-hosted hydrothermal sites, this weak or lack of magnetization can result from a combination of thermal demagnetization of titanomagnetite in the basalt [e.g., Kent and Gee, 1996], alteration of titanomagnetite to less magnetic minerals such as titanomaghemite by contact with the pervasive circulation of hot and reducing hydrothermal fluids [Ade-Hall *et al.*, 1971; Johnson and Pariso, 1987; Watkins and Paster, 1971; Tivey and Johnson, 2002; de Ronde *et al.*, 2011], and the progressive accumulation of a nonmagnetic hydrothermal deposit covering the underlying magnetized layer and increasing the distance between the magnetized basalt and the recording sensor, resulting in a decrease of the associated magnetic anomaly [Szitkar *et al.*, 2014].

Hydrothermal vent fields exist in other tectonic settings such as volcanic arcs [e.g., de Ronde *et al.*, 2001]; however, their geophysical characteristics are presently poorly constrained and the studies by Caratori Tontini *et al.* [2012a, 2014] so far remain the main contributions focusing on their magnetic properties. We use high-resolution vector magnetic data and associated high-resolution bathymetry collected by the German AUV *Abyss* during cruise POS442 of R/V *Poseidon* in October 2012 to investigate the magnetic signature of a volcanic-arc-related basalt-hosted massive sulfide occurrence located within a crater-shaped depression belonging to the Palinuro volcanic complex, in the southern Tyrrhenian Sea [Petersen *et al.*, 2014]. This depression is located on the eastern wall of the area surveyed by Caratori Tontini *et al.* [2014], and the associated hydrothermal site is in a waning phase, as no indications for active black smoker-type chimneys were observed either visually or as a plume signal in the water column. Weak, low temperature fluid discharge ($\sim 60^{\circ}\text{C}$) is present [Monecke *et al.*, 2009; Thiel *et al.*, 2012], suggesting that thermal demagnetization of the

uppermost basalt is unlikely although a deeper underlying heat source probably exists. We consider a nested forward modeling approach combined thermal modeling of the site to address the question of the shape and size of the nonmagnetic deposit and investigate the geometry of the underlying magnetized layer, revealing a surprisingly large stockwork zone extending laterally beyond the limits of the deposit beneath the three volcanic cones surrounding the depression.

2. Geological Settings

Despite accounting for roughly 26% of the Earth's magmatic budget [Perfit and Davidson, 2000], volcanic arcs only started to be extensively surveyed for hydrothermal mineralization in recent years [de Ronde *et al.*, 2001, 2012, 2014; Embley *et al.*, 2004; Resing *et al.*, 2007]. Although mid-ocean ridges and some volcanic-arc-related hydrothermal systems may share a common basaltic host, the volcanic arc systems exhibit specific characteristics such as a comparatively shallower depth, i.e., a weaker hydrostatic pressure [de Ronde *et al.*, 2005; Hannington *et al.*, 2005; Monecke *et al.*, 2014], allowing fluids to boil during their ascent to the seafloor and the existence of variably thick volcaniclastic coverage.

The Palinuro volcanic complex is an E-W trending volcanic chain whose tectonic origin is still debated [e.g., Colantoni *et al.*, 1981; Chiarabba *et al.*, 2008; Marani and Gamberi, 2004a; Del Ben *et al.*, 2008; Milia *et al.*, 2009; Passaro *et al.*, 2010; Milano *et al.*, 2012]. It is located in the Tyrrhenian Sea, at the northeastern end of the Aeolian volcanic arc, in the vicinity of Sicily (~100 km South) and Calabria (~50 km East) and extends over 70 km in length for a 25 km width, at depths reaching 3200 m at the base of its southern slope, whereas the northern one, reaching 1800 m, acts as a transition with the Calabrian continental shelf. The shallowest summits shoal to 70 m below the sea surface, forming two 10 and 3 km diameter flat plateaus, respectively (Figure 1a). Palinuro rocks are characterized by basaltic-andesitic compositions, similar to the Western Aeolian Seamounts [Trua *et al.*, 2004]. Unconsolidated volcaniclastic material have been recovered on Palinuro seamounts [Marani *et al.*, 1999] and confirmed by visual observations using ROV and TV-guided instruments [Petersen and Monecke, 2008]. However, sampling by dredging [Del Monte, 1972; Colantoni *et al.*, 1981] and drilling [Petersen and Monecke, 2009] recovered coherent lava of basaltic to basaltic-andesitic composition at various locations within the complex. These observations may be interpreted as an evidence for thin volcaniclastic coverage.

Along with other volcanoes of the Tyrrhenian Sea (namely Marsili and Panarea), the Palinuro complex shows evidence for hydrothermal activity [Lupton *et al.*, 2011], especially in its westernmost part. This westernmost sector is dominated by a half circular rim (4 km in diameter) with steep flanks probably related to caldera formation having occurred during the most recent stage of volcanic activity [Marani and Gamberi, 2004b; Ligi *et al.*, 2014] (Figure 1a). This western sector hosts hydrothermal activity and its associated seafloor sulfide and Mn-Fe oxide deposits are covered by a sedimentary layer [Minniti and Bonavia, 1984; Peters *et al.*, 2011; Petersen *et al.*, 2014]. Geophysical investigations of these hydrothermal sites were recently provided by Caratori Tontini *et al.* [2014] and Ligi *et al.* [2014]. The northeastern wall has a volcanic summit with three individual cones topping at 555 m below the sea level (Figures 1b and 2a) and enclosing the 750 m wide circular depression investigated in this study (Figure 1b). The above mentioned drilling program penetrated a partially buried sulfide-sulfate mineralization zone at the bottom of the depression (Figure 1b), revealing an accumulation of hydrothermal and volcaniclastic material [Petersen *et al.*, 2014]. Moreover, the high-resolution bathymetric grid provided by the AUV Abyss multibeam echo sounder in 2012 unveils two prominent features, potentially dikes, to the West and the Southwest of the depression but the computed RTP anomaly does not provide any evidence concerning their extension under the depression (Figures 1b and 2). It also reveals the presence of volcanic pinnacles located on the internal face of the northeastern cone (Figure 1c). The entire structure is characterized by a horseshoe shape opening to the Southeast (Figure 1b).

3. Data Acquisition and Processing

During cruise POS442 of R/V Poseidon in October 2012, high-resolution vector magnetic data were collected using GEOMARs AUV Abyss, a REMUS6000 system. In order to achieve a complete survey of the crater-shaped depression, the AUV followed 100 m spaced parallel profiles along an either ENE-WSW or NNW-SSE orientation, at an average altitude of 100 m above the seafloor (ranging from 30 to 165 m; Figures 1 and 2b) and acquired magnetic data at a 10 Hz frequency, allowing a very precise estimation of the magnetic anomaly. In

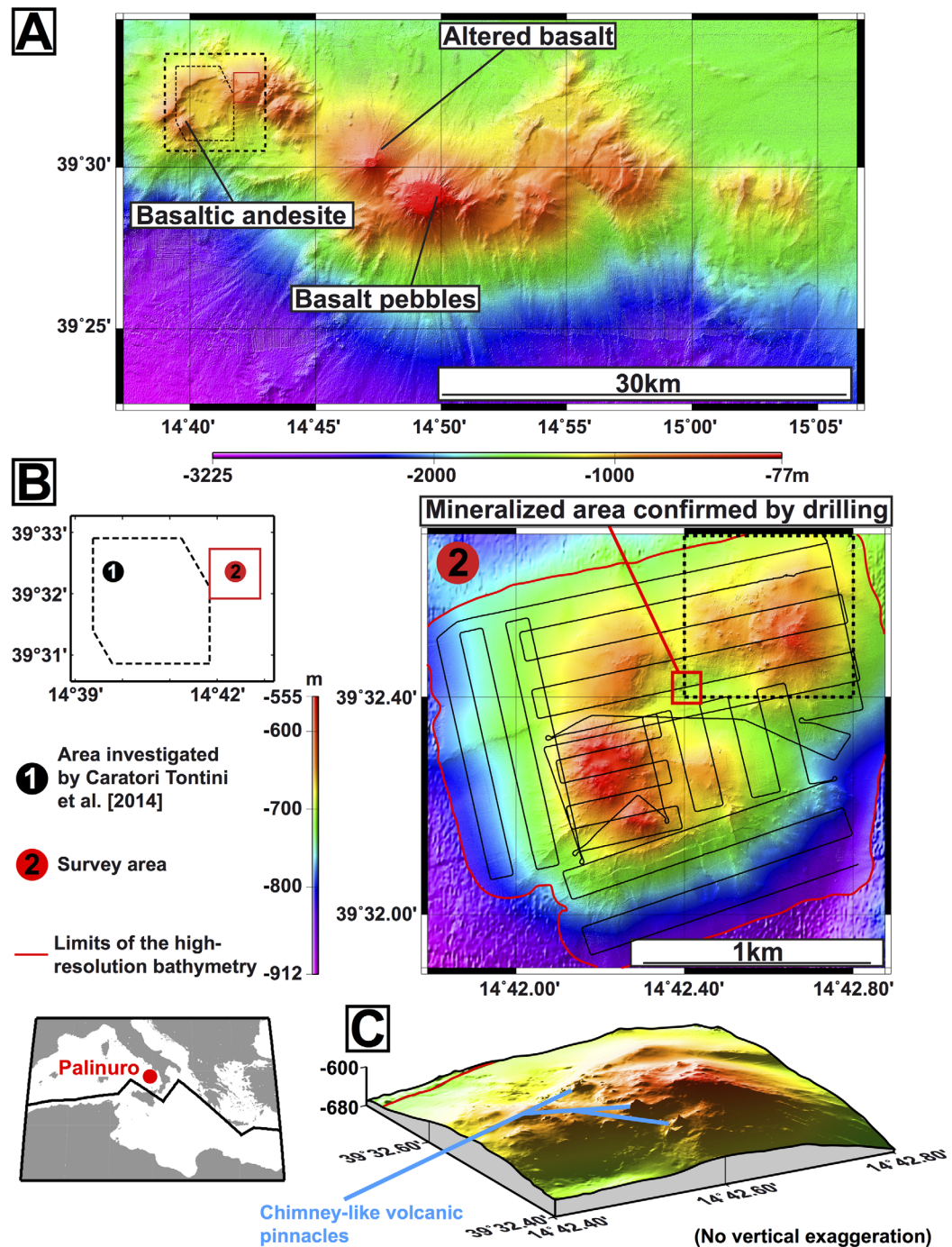


Figure 1. (a) Regional bathymetric map of the Palinuro volcanic complex. The studied area is surrounded by the red box and is located to the East of that investigated by Caratori Tontini et al. [2014]. (b) High-resolution bathymetric map of the crater-shaped depression. The black lines correspond to the AUV path whereas the dotted line encompasses the 3-D view presented in Figure 1c and revealing the presence of chimney-like volcanic pinnacles. The location of coherent volcanic rock samples recovered in the area is also given.

addition, high-resolution bathymetric data were collected using the AUV multibeam echo sounder, resulting in a bathymetric map gridded at 60 cm with a vertical resolution of 20 cm. These data are completed by a ship-based bathymetric grid (10 m grid with a vertical resolution of 3 m) provided by an EM122 multibeam echo sounder and acquired during R/V Meteor cruise M86/4 in early 2012 [Petersen, 2012].

Processing high-resolution magnetic data collected by a fluxgate magnetometer mounted to the frame of an underwater vehicle must be undertaken with care. Unlike surface measurements, where the

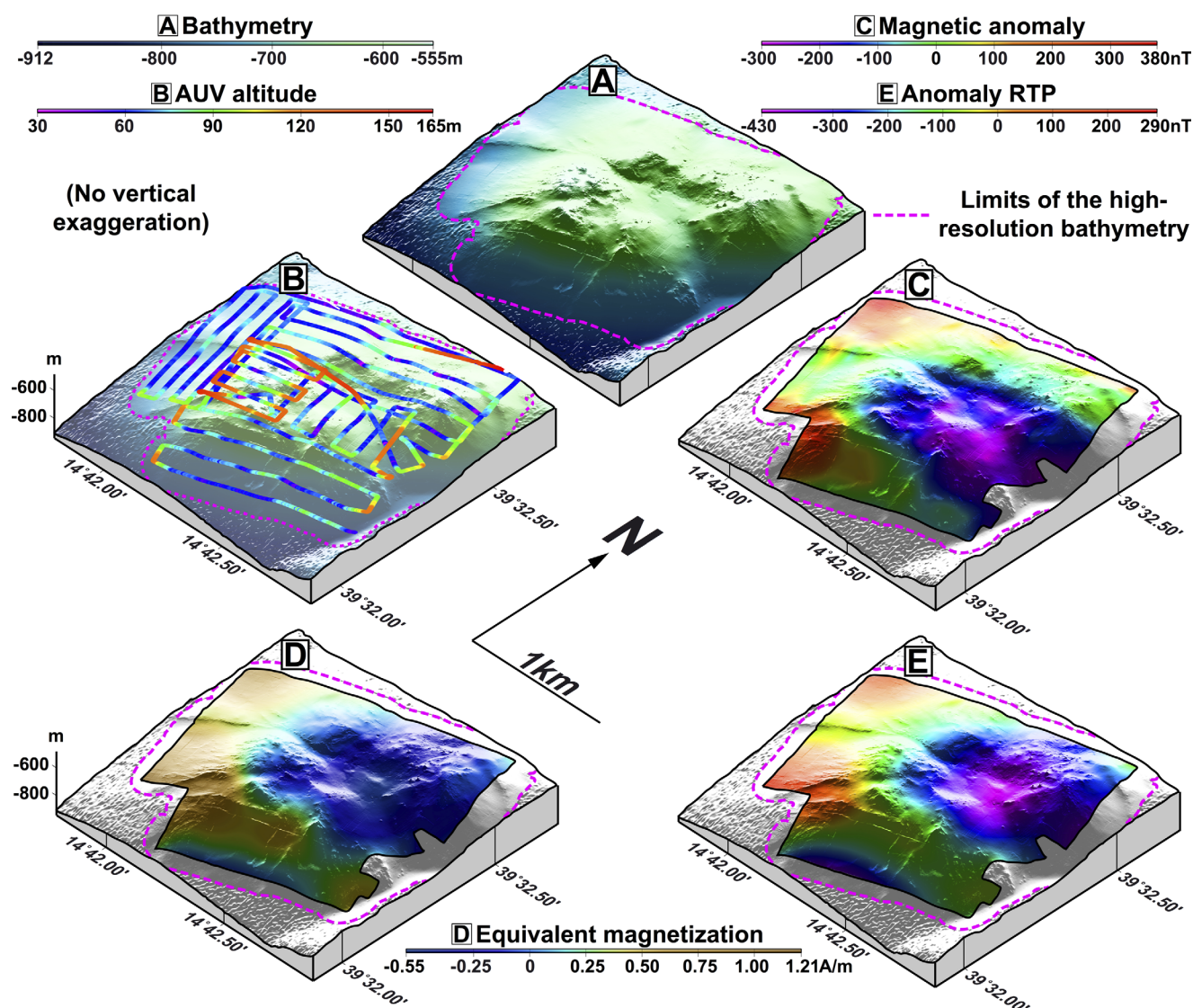


Figure 2. (a) Perspective view of the crater-shaped depression. The three bathymetric highs clearly appear. (b) Altitude of the AUV above the seafloor. The variations rule out the possibility to directly reduce the magnetic anomaly presented in Figure 2c to the pole. (d) Equivalent magnetization computed using the ABIC inversion method for a 500 m thick magnetized layer. (e) RTP anomaly recomputed from the equivalent magnetization and assuming a vertical geomagnetic field. The strongest negative values are centered above the nonmagnetic deposit.

magnetometer is towed at a sufficient distance to eliminate the magnetic influence of the ship, the immediate proximity of the underwater vehicle strongly affects the raw data. The magnetic influence of the AUV has therefore to be quantified and removed, in order to resolve the crustal magnetic anomaly.

The AUV magnetic susceptibility tensor (nine coefficients) and remanent magnetization vector (three coefficients) are estimated at the beginning of the dive, when the AUV is still at, or near the sea surface, using a method developed by Isezaki [1986] and Honsho *et al.* [2009]. The vehicle is then considered far enough from both the ship and the seafloor, so that the magnetic measurements should be equal to the Earth's magnetic field values (total field) predicted by the IGRF (International Geomagnetic Reference Field) [International Association of Geomagnetism and Aeronomy (IAGA) Working Group V-MOD, 2010]. Any variation from this assumption is seen as a consequence of the magnetic influence of the vehicle. In our case, the estimation of the coefficients is achieved thanks to a complex calibration pattern performed by the AUV at the beginning of its dive. This pattern is made of a succession of "figures-8's," allowing measurements of the magnetic field in all directions with roll variations but at zero pitch, followed by a combination of short ascents and descents in both N-S and E-W directions to estimate the effect of pitch variations at zero roll.

The resulting matrix data of magnetic components, first calculated in the AUV reference frame, is converted to geographical coordinates using the Euler rotation matrix, and transformed to vector magnetic anomaly by subtracting the geomagnetic field approximated by the IGRF [IAGA Working Group V-MOD, 2010]. The resulting magnetic anomaly is presented in Figure 2c and reveals a zone characterized by negative values to the East of the survey area, whereas the western part is characterized by positive values.

Nevertheless, the directionality inherent in magnetic fields (inclination and declination) results in magnetic anomalies being phase-shifted so that they are not centered over the causal body, unless the survey area is located at a magnetic pole. To replace the anomalies above their causative sources, a further processing step, called reduction to the pole (RTP), is required. This step consists of recalculating the measured anomalies assuming a vertical geomagnetic field (as if they were ideally acquired at the magnetic pole), in order to ease their interpretation. However, direct reduction to the pole is generally achieved in the spectral domain and requires data to be collected or reduced to a horizontal plane, but Figure 2b indicates strong altitude variations of the AUV, ruling out its application. Two options remain:

1. Upward-continuing the data to a datum plane located above the shallowest point of the survey [Guspi, 1987], although this approach results in a loss of short wavelengths, i.e., a reduced resolution.
2. Applying an equivalent source method, i.e., inverting the observed magnetic anomalies to equivalent magnetization from which we recompute the anomaly assuming vertical field and magnetization vectors [e.g., Szitkar et al., 2014] (Figure 2d). We use the inversion method developed by Honsho et al. [2012] based on the Akaike Bayesian Information Criterion (ABIC) which, unlike other inversion methods, is achieved along the uneven tracks of the vehicle in the space domain, i.e., it does not require the data to be acquired on a datum plane. In this method, the magnetization distribution is estimated by a linear combination of bicubic splines and we aim to determine their expansion coefficients. This inversion takes full advantage of the varying altitudes of the AUV above the seafloor and consequently allows conservation of the short wavelengths. As a result of the nonuniqueness of potential field solutions, an infinite number of solutions exist for magnetic inversions, regardless of the chosen method. The solutions are obtained by adding or removing a certain amount of annihilator [Parker and Huestis, 1974] (a magnetization distribution producing no magnetic anomaly in the geometry of the experiment), among which the most likely one is chosen based on geological or geophysical considerations. In our case, we search for an equivalent source which geological significance is of little interest, and therefore adopt the one resulting from the application of the Honsho et al. [2013] algorithm under the following hypotheses. The magnetized layer is assumed to be 500 m thick with the upper surface defined by the bathymetry, resulting in a magnetization distribution with a maximum contrast of 1.7 A/m (Figure 2d). With this result, we compute the anomaly assuming vertical field and magnetization vectors, obtaining a mathematically rigorous RTP anomaly (Figure 2e), which reveals that the area characterized by the strongest negative anomaly corresponds to the bottom of the crater-shaped depression covered by hydrothermal and volcaniclastic sediments. As volcanism in this area is younger than the last polarity reversal [Cocchi et al., 2009], this negative magnetic anomaly corresponds to a weak or lack of magnetization and not to a highly magnetized area with a reverse polarity.

4. Forward Modeling

By studying the magnetic anomaly, we aim to constrain both the shape and volume of the nonmagnetic deposit and the geometry of the underlying magnetized layer, providing crucial information concerning the characteristics of the stockwork and/or the heat source at depth. We adopt a forward modeling approach to estimate the influence of various hypotheses on the magnetic anomaly, until we reach a modeled anomaly comparable to that computed in Figure 2e.

Modeled magnetic anomalies result from a combination of three parameters: (1) the thickness of the magnetized layer, (2) the magnetization of the basalt, and (3) sediment cover (including a potential hydrothermal deposit) increasing the distance between the magnetized source and the magnetometer. An infinite number of linear combinations of these hypotheses consequently match the observed anomalies and it is therefore important to consider a nested approach, in order to keep physically and geologically reasonable hypotheses. It is also worth noting that we do not aim to systematically mimic second order anomalies, as

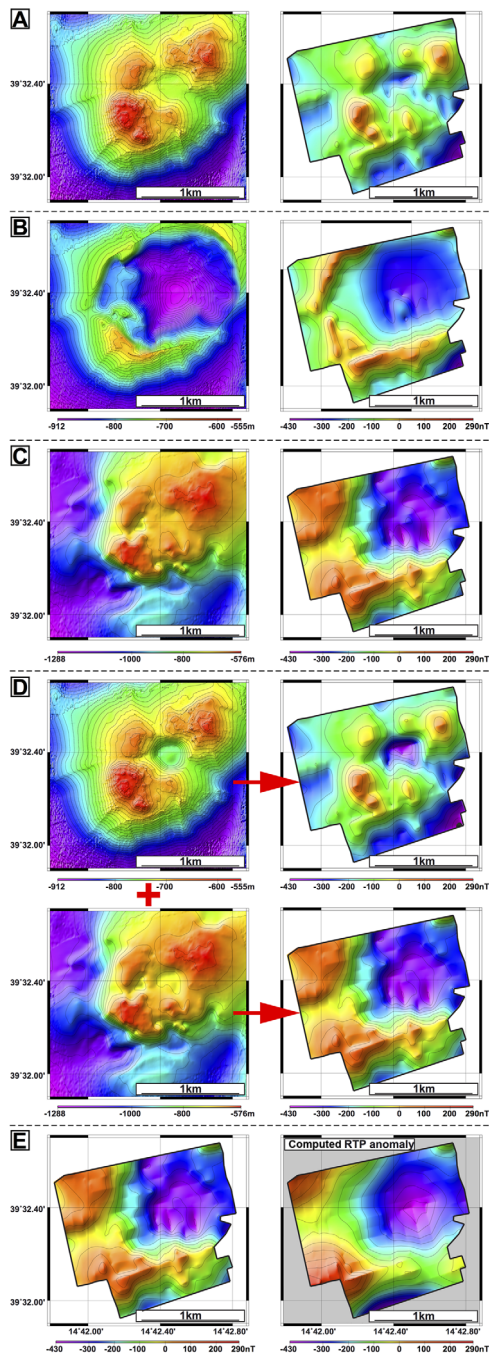


Figure 3. Comparison between synthetic anomalies and computed RTP (bottom right) (a) Modeled anomaly computed in the geometry of the experiment, assuming a 500 m thick, 1.7 A/m magnetized layer. The shape of the resulting synthetic anomaly does not match that of the RTP anomaly and generally follows the bathymetry. (b) Shape and thickness nonmagnetic material should have to match the computed RTP anomaly on a first order. Such deposit is far beyond reasonable with respect to the limited amount of volcaniclastic material observed throughout the volcanic chain. (c) Requested shape for the underlying magnetized layer to produce a satisfying modeled anomaly. This step does not take the influence of the non-magnetic deposit into account and is therefore not sufficient. (d) (top) High-resolution bathymetry including the shape of the nonmagnetic deposit obtained by downward-continuing the cone slopes under the sediment coverage and associated modeled anomaly. (bottom) Shape of the underlying magnetized layer which, combined with the nonmagnetic deposit, produces a satisfying modeled anomaly. (e) Comparison between modeled and computed RTP anomalies.

short wavelength variations may result from small sources, on which we lack reliable information. Trying to model such sources would likely result in making doubtful assumptions.

To generate the modeled anomaly, the 60 cm \times 60 cm high-resolution bathymetry is discretized into prisms with a 5 m \times 5 m square section and an infinite depth. Because of the average AUV altitude of 100 m above the seafloor, we extend the limits of the high-resolution bathymetry using the surface bathymetry provided by R/V Meteor to prevent any edge effect, and consider a 2 km \times 2 km square perimeter filled with 160,000 prisms (and no gaps) around each AUV observation point (X, Y, and Depth). As potential short wavelength variations of the magnetization intensity within the magnetized layer are not constrained, we consider a uniformly 1.7 A/m magnetized seafloor contrast resulting from the Bayesian inversion (Figure 2d). The magnetic influence of every prism forming the mesh of the model is calculated considering a 90° magnetization inclination and a 0° declination, producing a synthetic signal that can be compared to the RTP anomaly computed from the inversion. Considering the decrease of the magnetic anomaly amplitude with the cube of the distance, the magnetic influence of a prism located at the edge of the 2 km perimeter for the upper limit of the magnetized layer (i.e., the seafloor) is only 0.1% of that of a prism located under the AUV and is therefore negligible. For the lower limit (i.e., the base of the magnetized layer), the same calculation leads to a value of 13% of the prism located directly beneath the AUV, which remains acceptable, with respect to the much weaker magnetic anomalies generated by this interface (~5% of the influence of the upper interface). Assuming these hypotheses, it becomes possible to investigate consequences of thickness variations of both the nonmagnetic deposit and the underlying magnetized layer.

In all the following models, the calculation is done at the observation level of the AUV. This level is subject to variations, as revealed in Figure 2b, in order to adjust the position of the vehicle with respect to the local topography. Because the nature of the prominent features to the West and the Southwest of the depression remains speculative, as well as their extension under the depression, trying to take them into account would be extremely hazardous.

1. We test the effect of the bathymetry only, defining a 500 m thick magnetized layer, to remain consistent with the hypothesis chosen for the magnetic inversion. The result is presented in Figure 3a and reveals that the modeled anomaly follows the shape of the bathymetry, with positive values centered above the three volcanic cones surrounding the central depression. This result is interpreted as a consequence of the comparatively smaller altitude of the AUV above these areas, i.e., its closer proximity to the seafloor (Figure 2b). The general shape of this first modeled anomaly does not match the calculated RTP anomaly (Figure 2e), and its peak-to-peak amplitude is too weak, suggesting that additional sources must be taken into account.
2. We estimate the shape and size a mixture of nonmagnetic hydrothermal and volcaniclastic material should have to produce a satisfying modeled anomaly, without considering any variations of the underlying magnetized layer thickness. The characteristics of such deposit are defined, so that the magnetic influence of the three volcanic cones is eradicated. The result presented in Figure 3b reveals that the only way to get an anomaly roughly matching the RTP anomaly shape over the depression imposes to consider both an extremely large and deep deposit, largely exceeding that of sites with a comparable size [Humphris *et al.*, 1995; Hannington *et al.*, 1998]. As the hydrothermal area does not encompass the two western volcanic cones (no evidence of hydrothermal activity has been observed there), the western part of the crater-shaped depression should be made of a massive accumulation of volcaniclastic material, far beyond reasonable with respect to the observations throughout the volcanic chain. To the Northeast, evidence of only weak hydrothermalism does not support the hypothesis of a thick hydrothermal and volcaniclastic deposit on the cone flanks either. Moreover, the modeled anomaly does not match the RTP anomaly beyond the crater-shaped depression, especially to the West, where it remains too weak despite the lack of any deposit. This step therefore rules out nonmagnetic material as the only source of the RTP anomaly.
3. We now test the effect of a variably thick magnetized layer only. Indeed, the presence of hydrothermalism and associated massive sulfides-sulfates strongly suggests the existence of an area located beneath the site and hydrothermally altered by fluid circulation and/or heated above the Curie temperature of titanomagnetite ($\sim 200^{\circ}\text{C}$) by a deeper magma chamber [e.g., Kent and Gee, 1996], leading to thermal demagnetization (see below). Such an area can be related to a thinning of the magnetized layer under the hydrothermal site, where the hot hydrothermal fluids ascend to reach the seafloor. The result presented in Figure 3c is close to the RTP anomaly but remains unsufficient, as it does not allow quantifying the effect of the nonmagnetic deposit covering the center of the crater-shaped depression.
4. The final step consists in considering a well-constrained combination of the previous parameters, i.e., the effect of a nonmagnetic deposit locked between the three cones, as suggested by the bathymetry, and covering a variably thick magnetized layer. The strongest negative values of the RTP anomaly perfectly match the center of the crater-shaped depression (Figure 2) and the bathymetric map allows constraining the shape and dimensions of the corresponding nonmagnetic deposit with a downward-continuation of the cone slopes below the sediment coverage to determine the location and depth of their merging point. The role of such nonmagnetic deposit is estimated in Figure 3d (upper row) and the associated negative anomaly logically appears stronger than in Figure 3a, but the magnetic signature of the three cones still exists. As there is no reason to envisage consistent sediment coverage anywhere else, it finally becomes possible to constrain the shape of the underlying magnetized layer, confirming that a large nonmagnetic area extending under the cones is required. The shape of the underlying magnetized layer is presented in Figure 3d (lower row), along with the modeled anomaly produced by a combination of this variably thick layer and the nonmagnetic deposit. Figures 3e and 4 summarize our nested approach by comparing the final modeled anomaly with the computed RTP anomaly and displaying 3-D views of the deep structure of the site.

5. Discussion

The magnetized layer thickness chosen for the Bayesian inversion remains a matter of discussion. However, the line spacing of the survey and the average altitude of the measurements combined with the rapid decrease of the anomaly intensity with distance suggest that any thickness of more than several hundred meters would not have a noticeable impact on the magnetization contrast. Moreover, even if this thickness

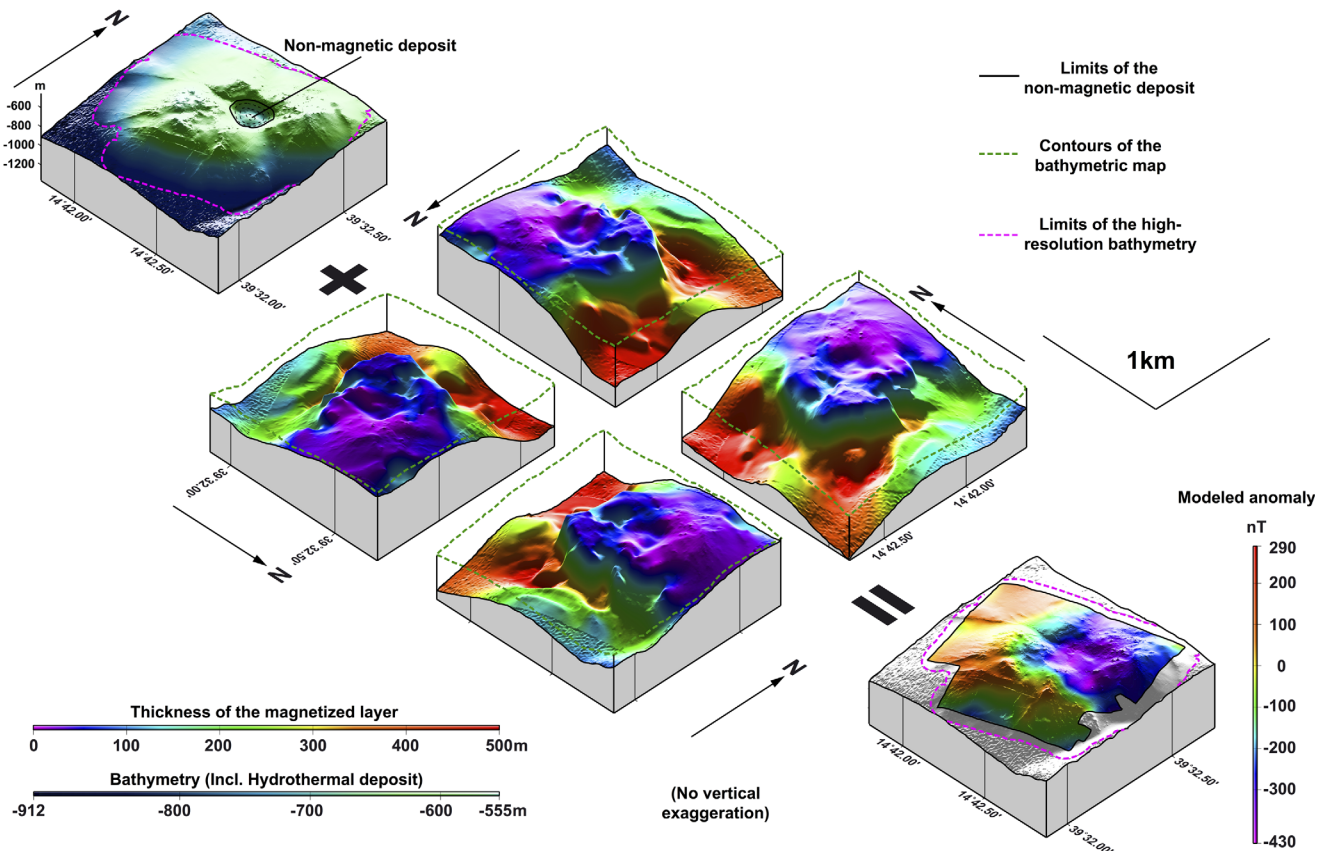


Figure 4. Perspective view of the crater-shaped depression, taking the hydrothermal occurrences into account and thickness of the underlying magnetized layer (shown are various angles), leading to the final modeled anomaly.

remains uncertain, it does not have any influence on the shape of the observed RTP anomaly and the only difference concerns its peak-to-peak amplitude, which slightly varies. While the 500 m value could be an arbitrary estimate for the thickness of the magnetized layer based on previous magnetic studies of arc volcanoes [Caratori Tontini *et al.*, 2012a, 2012b], the inversion model resolution is not particularly sensitive to reasonable variations of this parameter (4.6% of variations for a thickness varying from 300 to 500 m), with little impact on the conclusion related to the shape of the hydrothermal deposit and the geometry of the stockwork zone.

Assuming our hypotheses, we roughly estimate the volume of Palinuro's nonmagnetic deposit. Figure 1b and 3 suggest a deposit with a roughly conic shape pointing downward (circular base with a 400 m diameter). Moreover, the downward-continuation of the cone slopes reveals that their merging point is located 50 m below the top of the sediment coverage. Simple calculation allows estimating a volume of $\sim 2 \times 10^6$ m³, comparable to that of other basalt-hosted hydrothermal sites [e.g., Humphris *et al.*, 1995; Hannington *et al.*, 1998].

The forward modeling approach reveals that the zone characterized by a thinner magnetized layer expands beyond the limits of the known nonmagnetic deposit (Figures 3–5). Such geometry is interpreted as an altered and/or hot zone below the bathymetric highs surrounding the depression (Figure 5) and these "lobes" extending upward may be a consequence of older volcanic episodes having altered or heated the underlying magnetized layer above the Curie temperature of titanomagnetite.

To discriminate among these hypotheses, we compute a 3-D thermal model with the open KWare Heat3D geophysical heat flow simulator. The code models the thermal state by finite difference solution of energy and momentum conservation equations (i.e., Navier-Stokes) [Wohletz *et al.*, 1999]. These equations express heat transfer by conduction and convection with nonlinearities arising from variations of thermal conductivity within a heterogeneous material and heat sources/sinks (e.g., latency). We assume the existence of a

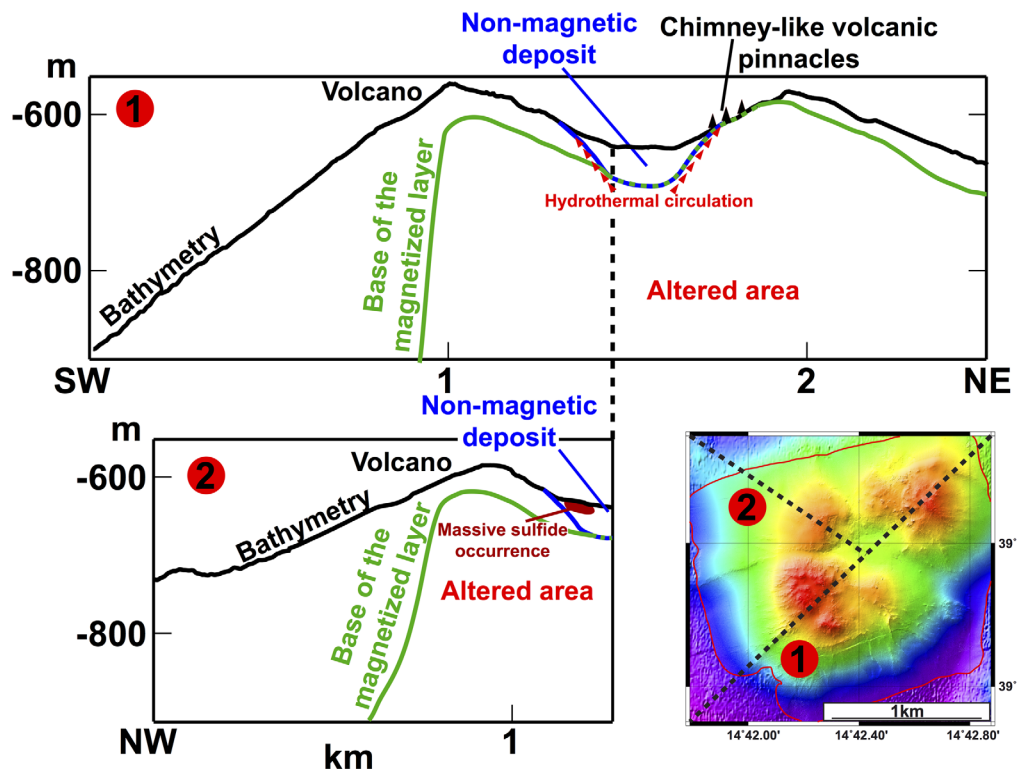


Figure 5. Schematic representation of the deep structure of the Palinuro hydrothermal site along two profiles. (top) SW-NE profile cutting across the two main bathymetric highs. (bottom) Additional NW-SE profile cutting across the smaller cone located to the Northwest of the crater-shaped depression and drilled massive sulfide-sulfate occurrence. The two profiles correspond to the dotted black lines on the bathymetric map. The particular geometry of the magnetized layer is interpreted as a consequence of older volcanic episodes having generated the three cones surrounding the depression and altered the underlying magnetized layer. The presence of hydrothermal discharge next to the observed chimney-like volcanic pinnacles on the internal face of the northeastern cone supports the hypothesis of a complete eradication of the underlying magnetized layer.

cooling heat source at depth, transferring the heat to other layers by conduction and evaluate its characteristics, so that the lower magnetized interface corresponds to a thermal demagnetization of titanomagnetite. Assuming a basaltic-andesite lithology forming the area of interest, we consider the following parameters: (1) Heat source with a melting temperature of 1200°C, density of 3000 kg/m³, thermal conductivity $K = 1.8 \text{ W}/(\text{mK})$, specific heat $C_p = 1.2 \text{ J}/(\text{kg K})$; (2) Basalt-andesite host rocks having a density of 2750 kg/m³, thermal conductivity $K = 2.6 \text{ W}/(\text{mK})$, specific heat $C_p = 910 \text{ J}/(\text{kg K})$ [Sleep, 1975; Parker and Oldenburg, 1973]. Both the bathymetry and the base of the magnetized layer are discretized into prisms with a 100 m × 100 m square section and we surmise the presence of a 2000 year old heat source 1000 m below the seafloor (Figure 6a)—which is considered as a minimum reasonable depth—in order to investigate the cooling process. During the first 1000 years (Figure 6b), the isotherms follow the shape of the intrusion with a steep heat gradient, the temperature decreasing from 1200°C within the intrusion to 250°C in 100–200 m. On the longer term, the isotherms become progressively smoother. The last cooling step appears to be the most consistent with the current situation, as the lack of active high-temperature discharge (e.g., black smokers) rules out the presence of an active heat source at depth. With this heat source, thermal demagnetization of titanomagnetite in the basalt would only occur at depths of ~800 m below the seafloor, i.e., much deeper than the lower base of the magnetized layer. To get a thermal demagnetization consistent with the base of the magnetized layer, the heat source would have to be located at an unrealistic shallow depth, suggesting that the base of the magnetized layer likely results from alteration of titanomagnetite rather than thermal demagnetization. Moreover, on the northeastern volcanic cone, this base is located immediately below the volcanic pinnacles, supporting the hypothesis of an alteration of magnetized material resulting from volcanic activity (Figure 5).

The lower limit of the stockwork remains ambiguous and would require further exploration such as ODP/IODP deep drilling. It remains therefore possible that the vertical heat gradient, although relatively weak,

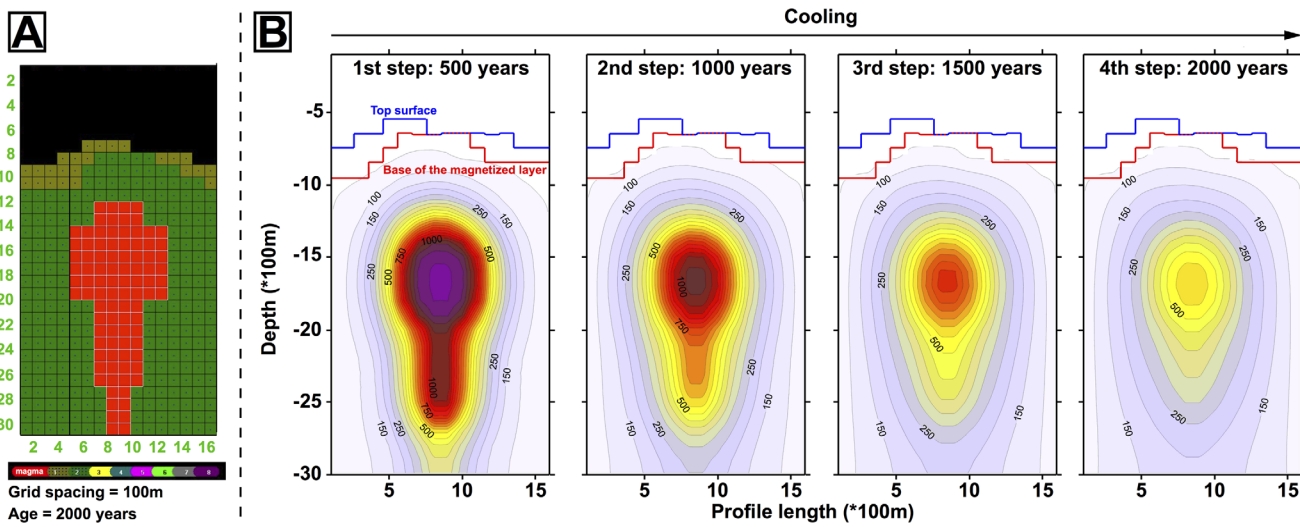


Figure 6. Thermal modeling of the site. (a) Assumed heat source corresponding to a magma chamber located ~1000 m below the seafloor and characterized by a 1200°C temperature within the intrusion. (b) Progressive cooling of the source with time. The lack of active chimneys on the seafloor suggests that the fourth step of the process is the most likely, but rules out the hypothesis of thermal demagnetization as a significant contributor for the specific magnetic signature of the site.

could lead to a thermal demagnetization at greater depths, possibly resulting from an ascending hydrothermal pipe beneath the site [e.g., Sztikar and Dymant, 2015].

6. Conclusions

Like all other basalt-hosted hydrothermal sites investigated to date, the volcanic-arc-related basalt-hosted hydrothermal site Palinuro exhibits a strong negative magnetic anomaly, i.e., a lack of magnetization. This specific magnetic signature, combined with a nested forward modeling approach and thermal modeling allows structurally constraining the deeper parts of the volcano. Our study reveals that the nonmagnetic deposit associated with the site cannot account for the observed anomaly, suggesting variations in the thickness of the magnetized layer at the site. This thin magnetized layer laterally extends beyond the limits of the non-magnetic deposit and provides insight into the location of a stockwork zone that forms lobes under the flanks of the volcano. These lobes are believed to be a consequence of older volcanic episodes having created the cones surrounding the depression and largely altered underlying magnetized layers. To the Northeast, the presence of hydrothermal discharge located next to the volcanic pinnacles also concurred to increase this alteration process by totally eradicating the magnetized crust under the internal face of the cone.

Acknowledgments

AUV data such as bathymetry and magnetic raw data as well as processed data will be archived on dedicated servers by the Kiel Data Management Team (KDMT) in GEOMARs Ocean Science Information System (OSIS-Kiel). Contact information for access to these large volume data files and metadata information will be provided by the central OSIS-Kiel (<https://portals.geomar.de/osis>). We thank the captain and crew of R/V Poseidon and the technical team of AUV Abyss for excellent work at sea. We gratefully thank M. Tivey and the anonymous reviewer, who largely concurred to improve this manuscript. We also thank N. Augustin and A. Steinbücher for having processed the high-resolution bathymetric data used in this study. Chie Honsha deserves our gratitude for offering us the opportunity to use her ABIC inversion method to perform the reduction to the pole. **GEOMAR, Helmholtz Centre for Ocean Research (Kiel, Germany)** supported this research.

References

- Ade-Hall, J. M., H. C. Palmer, and T. P. Hubbard (1971), The magnetic and opaque petrological response of basalt to regional hydrothermal alteration, *Geophys. J. R. Astron. Soc.*, **24**, 137–174.
- Caratori Tontini, F., B. Davy, C. E. J. de Ronde, R. W. Embley, M. Leybourne, and M. A. Tivey (2012a), Crustal magnetization of Brothers Volcano, New Zealand, measured by autonomous underwater vehicles: Geophysical expression of a submarine hydrothermal system, *Econ. Geol.*, **107**, 1571–1581, doi:10.2113/econgeo.107.8.1571.
- Caratori Tontini, F., C. E. J. de Ronde, D. Yoerger, J. Kinsey, and M. Tivey (2012b), 3-D focused inversion of near-seafloor magnetic data with application to the Brothers volcano hydrothermal system, southern Pacific Ocean, New Zealand, *J. Geophys. Res.*, **117**, B10102, doi: 10.1029/2012JB009349.
- Caratori Tontini, F., G. Bortoluzzi, C. Carmisciano, L. Cocchi, C. E. J. de Ronde, M. Ligi, and F. Muccini (2014), Near-bottom magnetic signatures of submarine hydrothermal systems at Marsili and Palinuro Volcanoes, Southern Tyrrhenian Sea, Italy, *Econ. Geol.*, **109**, 2119–2128.
- Chiarabba, C., P. De Gori, and F. Speranza (2008), The southern Tyrrhenian subduction zone: Deep geometry, magmatism and Plio-Pleistocene evolution, *Earth Planet. Sci. Lett.*, **268**, 408–423.
- Cocchi, L., F. Caratori Tontini, F. Muccini, M. P. Marani, G. Bortoluzzi, and C. Carmisciano (2009), Chronology of the transition from a spreading ridge to an accretional seamount in the Marsili backarc basin (Tyrrhenian Sea), *Terra Nova*, **21**, 369–374.
- Colantoni, P., F. Lucchini, P. L. Rossi, R. Sartori, and C. Savelli (1981), The Palinuro volcano and magmatism of the southeastern Tyrrhenian Sea (Mediterranean), *Mar. Geol.*, **39**, M1–M12.
- Del Ben, A., C. Barnaba, and A. Tobaga (2008), Strike-slip systems as the main tectonic features in the Plio-Quaternary kinematics of the Calabrian arc, *Mar. Geophys. Res.*, **29**, 1–12.
- Del Monte, M. (1972), Il vulcanesimo del Mar Tirreno: Nota preliminare sui vulcani Marsili e Palinuro, *Giornale Geol.*, **38**, 231–252.

- de Ronde, C. E. J., E. T. Baker, G. J. Massoth, J. E. Lupton, I. C. Wright, R. A. Feely, and R. R. Greene (2001), Intra-oceanic subduction-related hydrothermal venting, Kermadec volcanic arc, New Zealand, *Earth Plant. Sci. Lett.*, 193(3–4), 359–369.
- de Ronde, C. E. J., et al. (2005), Evolution of a submarine magmatic hydrothermal system: Brothers Volcano, Southern Kermadec Arc, New Zealand, *Econ. Geol.*, 100, 1097–1133.
- de Ronde, C. E. J., et al. (2011), Submarine hydrothermal activity and gold-rich mineralization at Brothers volcano, Kermadec arc, New Zealand, *Miner. Deposita*, 46, 541–584, doi:10.1007/s00126-011-0345-8.
- de Ronde, C. E. J., D. A. Butterfield, and M. I. Leybourne (2012), Metallogenesis and mineralization of intraoceanic arcs I: Kermadec Arc—Introduction, *Econ. Geol.*, 107, 1521–1525.
- de Ronde, C. E. J., J. R. Hein, and D. A. Butterfield (2014), Metallogenesis and mineralization of intraoceanic arcs II: The Aeolian, Izu-Bonin, Mariana, and Kermadec arcs, and the Manus backarc basin—Introduction, *Econ. Geol.*, 109, 2073–2077.
- Embley, R. W., E. T. Baker, W. W. Chadwick Jr., J. E. Lupton J. A. Resing, G. L. Massoth, and K. Nakamura (2004), Explorations of Mariana arc volcanoes reveal new hydrothermal systems, *Eos Trans. AGU*, 85, 37–44.
- Guspi, F. (1987), Frequency-domain reduction of potential field measurements to a horizontal plane, *Geoexploration*, 24, 87–98, doi:10.1016/0016-7142(87)90083-4.
- Hannington, M. D., A. G. Galley, P. M. Herzig, and S. Petersen (1998), Comparison of the TAG mound and stockwork complex with Cyprus-type massive sulfide deposits, in *Proceedings of the Ocean Drilling Program, Scientific Results*, vol. 158, edited by P. M. Herzig et al., pp. 389–415, Ocean Drill. Program, College Station, Tex.
- Hannington, M. D., C. E. J. de Ronde, and S. Petersen (2005), Sea-floor tectonics and submarine hydrothermal systems, in *Economic Geology 100th Anniversary Volume*, edited by J. W. Hedenquist (Colorado School of Mines, United States), et al. pp. 111–141, Society of Economic Geologists Inc, Littleton, Colo.
- Honsho, C., J. Dymnt, K. Tamaki, M. Ravilly, H. Horen, and P. Gente (2009), Magnetic structure of a slow spreading ridge segment: Insight from near-bottom magnetic measurements onboard a submersible, *J. Geophys. Res.*, 114, B05101, doi:10.1029/2008JB005915.
- Honsho, C., T. Ura, and K. Tamaki (2012), The inversion of deep-sea magnetic anomalies using Akaike's Bayesian information criterion, *J. Geophys. Res.*, 117, B01105, doi:10.1029/2011JB008611.
- Honsho, C., T. Ura, and K. Kim (2013), Deep-sea magnetic vector anomalies over the Hakurei hydrothermal field and the Bayonnaise knoll caldera, Izu-Ogasawara arc, Japan, *J. Geophys. Res.*, 118, 5147–5164, doi:10.1002/jgrb.50382.
- Humphris, S. E., et al. (1995), The internal structure of an active sea-floor massive sulfide deposit, *Nature*, 377, 713–716.
- International Association of Geomagnetism and Aeronomy (IAGA) Working Group V-MOD (2010), International geomagnetic reference field: The eleventh generation, *Geophys. J. Int.*, 183, 1216–1230, doi:10.1111/j.1365-246X.2010.04804.x.
- Isezaki, N. (1986), A new shipboard three-component magnetometer, *Geophysics*, 51, 1992–1998.
- Johnson, H. P., and J. E. Pariso (1987), The effects of hydrothermal alteration on the magnetic properties of oceanic crust: Results from drill holes CY-2 and CY-2a, in *Cyprus Crustal Study Project: Initial Report, Holes CY2 and 2a*, edited by P. T. Robinson, I. L. Gibson and A. Panayiotou, *Geol. Surv. Can. Pap.* 85–29, pp. 283–293.
- Kent, D. V., and J. Gee (1996), Magnetic alteration of zero-age oceanic basalt, *Geology*, 24, 703–706.
- Ligi, M., L. Cocchi, G. Bortoluzzi, F. D'Orlano, F. Muccini, F. Caratori Tontini, C. E. J. de Ronde, and C. Carmisciano (2014), Mapping of seafloor hydrothermally altered rocks using geophysical methods; Marsili and Palinuro seamounts, southern Tyrrhenian Sea, *Econ. Geol.*, 109(8), 2103–2117.
- Lupton, J., et al. (2011), Active hydrothermal discharge on the submarine Aeolian arc, *J. Geophys. Res.*, 116, B02102, doi:10.1029/2010JB007738.
- Marani, M. P., and F. Gamberi (2004a), Structural framework of the Tyrrhenian Sea unveiled by seafloor morphology, *Mem. Descr. Carta Geol. Ital.*, 64, 97–108.
- Marani, M. P., and F. Gamberi (2004b), Distribution and nature of submarine volcanic landforms in the Tyrrhenian Sea: The arc vs. the back-arc: Agenzia per la Protezione dell'Ambiente e per i servizi Tecnici (APAT), *Mem. Descr. Carta Geol. Ital.*, 64, 109–126.
- Marani, P., F. Gamberi, L. Casoni, G. Carrara, V. Landuzzi, M. Musacchio, D. Penitenti, L. Rossi, and T. Trua (1999), New rock and hydrothermal samples from the southern Tyrrhenian Sea: The MAR-98 research cruise, *Giornale Geol.*, 61, 3–24.
- Milano, G., S. Passaro, and M. Sprovieri (2012), Present-day knowledge on the Palinuro seamount (south-eastern Tyrrhenian Sea), *Boll. Geofis. Teor. Appl.*, 53, 403–416, doi:10.4430/bgta0042.
- Milia, A., E. Turco, P. P. Pierantoni, and A. Schettino (2009), Four-dimensional tectono-stratigraphic evolution of the southeastern peri-Tyrrhenian basin (Margin of Calabria, Italy), *Tectonophysics*, 476, 41–56, doi:10.1016/j.tecto.2009.02.30.
- Minniti, M., and F. Bonavia (1984), Copper-ore grade hydrothermal mineralization discovered in a seamount in the Tyrrhenian Sea (Mediterranean): Is the mineralization related to porphyry copper or to base metal lodes?, *Mar. Geol.*, 59, 271–282.
- Monecke, T., S. Petersen, K. Lackschewitz, M. Hiegler, M. D. Hannington, and J. Bruce Gemmell (2009), Shallow submarine hydrothermal systems in the Aeolian volcanic arc, Italy, *Eos Trans. AGU*, 90(13), 110–111.
- Monecke, T., S. Petersen, and M. D. Hannington (2014), Constraints on water depth of massive sulfide formation: Evidence from modern seafloor hydrothermal systems in arc-related settings, *Econ. Geol.*, 109, 2079–2101.
- Nakamura, K., T. Toki, N. Mochizuki, M. Asada, J. Ishibashi, Y. Nogi, S. Yoshikawa, J. Miyazaki, and K. Okino (2013), Discovery of a new hydrothermal vent based on an underwater, high-resolution geophysical survey, *Deep Sea Res., Part I*, 74, 1–10.
- Parker, P., and D. Oldenburg (1973), Thermal model of an ocean ridge, *Nat. Phys. Sci.*, 242, 137–139, doi:10.1038/physci242137a0.
- Parker, R. L., and S. P. Huestis (1974), The inversion of magnetic anomalies in the presence of topography, *J. Geophys. Res.*, 79, 1587–1593.
- Passaro, S., G. Milano, C. D'Isanto, S. Ruggieri, R. Tonielli, P. Bruno, M. Sprovieri, and E. Marsella (2010), DTM-based morphometry of the Palinuro seamount (Italy, Eastern Tyrrhenian Sea): Geomorphological and volcanological implication, *Geomorphology*, 115, 129–140.
- Perfit, M. R., and J. P. Davidson (2000), Plate tectonics and volcanism, in *Encyclopedia of Volcanoes*, edited by H. Sigurdsson et al., pp. 89–113, Academic, San Diego, Calif.
- Peters, M., H. Strauss, S. Petersen, N. Kummer, and C. Thomazo (2011), Hydrothermalism in the Tyrrhenian Sea: Inorganic and microbial sulfur cycling as revealed by geochemical and multiple sulfur isotope data, *Chem. Geol.*, 280, 217–231.
- Petersen, S. (2012), Cruise report R/V Meteor cruise M86/4—Geological setting, pore water chemistry, sediment chemistry, and metagenomics of hydrothermal systems in the Tyrrhenian Sea, Leitstelle Dtsch. Forsch. METEOR Ber, M86/4, Hamburg, Germany.
- Petersen, S., and T. Monecke (2008), Cruise report R/V Poseidon cruise POS340—"TYMAS" Tyrrhenian Sea massive sulfides, IFM-GEOGRAPH Rep. 21, 77 pp., IFM-GEOMAR, Kiel, Germany.
- Petersen, S., and T. Monecke (2009), Cruise report R/V Meteor cruise M73/2—Shallow drilling of hydrothermal sites in the Tyrrhenian Sea (Palindrill), IFM-GEOGRAPH Rep. 30, 235 pp., IFM-GEOMAR, Kiel, Germany.

- Petersen, S., et al. (2014), Drilling shallow-water massive sulfides at the Palinuro Volcanic Complex, Aeolian Island Arc, Italy, *Econ. Geol.*, **109**, 2129–2157.
- Resing, J. A., G. Lebon, E. T. Baker, J. E. Lupton, R. W. Embley, G. J. Massoth, W. W. Chadwick Jr., and C. E. J. de Ronde (2007), Venting of acid-sulfate fluids in a high-sulfidation setting at NW Rota-1 submarine volcano on the Mariana arc, *Econ. Geol.*, **102**, 1047–1061.
- Sleep, N. H. (1975), Formation of oceanic crust: Some thermal constraints, *J. Geophys. Res.*, **80**, 4037–4042.
- Szitkar, F., and J. Dymnt (2015), Near-seafloor magnetics reveal tectonic rotation and deep structure at TAG (Trans-Atlantic Geotraverse) hydrothermal site (Mid-Atlantic Ridge, 26°N), *Geology*, **43**, 87–90, doi:10.1130/G36086.1.
- Szitkar, F., J. Dymnt, Y. Fouquet, and Y. Choi (2014), What causes low magnetization at basalt-hosted hydrothermal sites? Insights from inactive site Krasnov (MAR 16°38'N), *Geochem. Geophys. Geosyst.*, **15**, 1441–1451, doi:10.1002/2014GC005284.
- Thiel, V., et al. (2012), Widespread occurrence of two carbon fixation pathways in tubeworm endosymbionts: Lessons from hydrothermal vent associated tubeworms from the Mediterranean Sea, *Front. Microbiol.*, **3**, 1–20, doi:10.3389/fmicb.2012.00423.
- Tivey, M. A., and J. Dymnt (2010), The magnetic signature of hydrothermal systems in slow-spreading environments, in *Diversity of Hydrothermal Systems on Slow Spreading Ocean Ridges*, AGU Geophys. Monogr., vol. 188, edited by P. A. Rona et al., pp. 43–66, AGU, Washington, D. C., doi:10.1029/2008GM000773.
- Tivey, M. A., and H. P. Johnson (2002), Crustal magnetization reveals subsurface structure of Juan de Fuca Ridge hydrothermal vent fields, *Geology*, **30**, 979–982, doi:10.1130/0091-7613 (2002)030<0979:CMRSSO>2.0.CO;2.
- Tivey, M. A., P. A. Rona, and H. Schouten (1993), Reduced crustal magnetization beneath the active sulfide mound, TAG hydrothermal field, Mid-Atlantic Ridge, at 26°N, *Earth Planet. Sci. Lett.*, **115**, 101–115, doi:10.1016/0012-821X (93)90216-V.
- Trua, T., G. Serri, and P. L. Rossi (2004), Coexistence of IAB-type and OIB-type magmas in the southern Tyrrhenian back-arc basin: Evidence from recent seafloor sampling and geodynamic implications, *Mem. Descr. Carta Geol. Ital.*, **XLIV**, 83–96.
- Watkins, N. D., and T. P. Paster (1971), The magnetic properties of igneous rocks from the ocean floor, *Philos. Trans. R. Soc. London*, **268**, 507–550.
- Wohletz, K., L. Civetta, and G. Orsi (1999), Thermal evolution of the Phlegraean magmatic system, *J. Volcanol. Geotherm. Res.*, **91**, 381–414.
- Zhu, J., J. Lin, Y. J. Chen, C. Tao, C. R. German, D. R. Yoerger, and M. A. Tivey (2010), A reduced crustal magnetization zone near the first observed active hydrothermal vent field on the Southwest Indian Ridge, *Geophys. Res. Lett.*, **37**, L18303, doi:10.1029/2010GL043542.